

COMBINED MODE CRACK EXTENSION
IN ADHESIVE JOINTS

by

G. G. Trantina

Contract No. N00019-71-C-0323

Department of the Navy

Naval Air Systems Command

This document has been approved for
public release and sale, its distribution is unlimited.

Department of Theoretical and Applied Mechanics

University of Illinois at Urbana-Champaign

November, 1971

ABSTRACT

This study investigates crack extension in an adhesive system under combined mode loading. A finite element stress analysis for a slant edge-cracked plate furnishes the opening and shear mode stress intensity factors, K_I and K_{II} , over a wide range of slant angles and crack lengths. By varying the angle between the adhesive layer and the load line in a SEN specimen, combined mode crack extension is observed and the combined mode fracture toughness values are then determined. The effect of the location of the crack tip (center of bond or interface) is also discussed.

ACKNOWLEDGMENT

This investigation was conducted in the Department of Theoretical and Applied Mechanics at the University of Illinois. The author wishes to express his appreciation to his advisor, Professor H. T. Corten, for suggestions, constructive criticism, and encouragement. The assistance of H. T. James, Jr. and Mrs. R. A. Mathine in the preparation of the manuscript is gratefully appreciated.

Financial support for the study has been provided by the Naval Air System Command (Contract No. N00019-71-C-0323).

The results of this investigation are contained in Part Two of the author's Ph. D. thesis.

TABLE OF CONTENTS

	Page
INTRODUCTION	1
FRACTURE MECHANICS BACKGROUND.	2
FINITE ELEMENT ANALYSIS	5
General Procedure.	5
General Results	7
Results of Displacement Method	8
EXPERIMENTAL PROGRAM	9
Experimental Procedure and Results	9
Discussion of Results	12
SUMMARY AND CONCLUSIONS	14
REFERENCES	15
TABLES	17
FIGURES	23

INTRODUCTION

Structural adhesive bonds can be divided into two general categories-- composite materials consisting of fibers or particles bonded together by an adhesive matrix and structural components bonded together with an adhesive material. Three types of simple structural joints are shown in Fig. 1. Since adhesives are relatively brittle materials that inherently contain flaws, their fracture behavior can be readily described by the techniques of fracture mechanics.

A large number of variables influence the load carrying capabilities of an adhesive joint. Manufacturing variables include composition and preparation of adhesives and adherends and joint geometry. Variables imposed by service conditions include load history, environment, and stress mode (Fig. 2). A combined stress mode--mode I (opening) and mode II (forward sliding)--is considered in this paper.

Combined mode stress conditions are present in a number of adhesive joint configurations. Cracks in composite materials are often oriented such that a combined mode stress state exists. Combined mode stress conditions are present in the lap and scarf joints shown in Fig. 1. Even though cracks tend to grow into the mode I condition from a combined mode condition, in certain adhesive joint systems the combined mode state continues even as the crack extends.

The problem of the combined mode crack extension in the slant adhesive layer of a single-edge-notch (SEN) specimen was investigated. A finite element analysis was used to obtain the stress analysis and the mode I strain energy rate, \mathcal{G}_I , and the mode II strain energy rate, \mathcal{G}_{II} , for a homogeneous tension plate with a slant SEN. By utilizing the approximation (1) that for a very thin adhesive layer \mathcal{G} for the two-material system is approximately equal to \mathcal{G} for the one-material system and the experimental results for crack extension in the slant adhesive layer of SEN (aluminum-epoxy-aluminum) specimens, a diagram of \mathcal{G}_I versus \mathcal{G}_{II} at crack extension was obtained.

FRACTURE MECHANICS BACKGROUND

A general review of fracture mechanics concepts as well as a discussion of some of the literature concerned with adhesive systems under opening mode loading is included in Ref. (1). Consequently, this section will deal only with combined mode fracture studies and fracture criteria.

In 1957, Irwin (2) presented a criterion for predicting the path of an extending crack. He stated, "...that a crack moves along a path normal to the direction of greatest tension, so that the component of shear stress resolved on the line of expected extension of the crack is zero." Using large, center-cracked plexiglas plates, Erdogan and Sih (3) have presented results to support this hypothesis and have observed that, in ideal brittle materials, the "sliding" and "tearing" modes of crack extension did not take place. The observed mode of fracture was always a crack opening. They have also presented a fracture hypothesis based on the Griffith theory and restated the criterion as follows: "The crack will grow in the direction along which the elastic energy release per unit crack extension will be maximum and the crack will start to grow when this energy reaches a critical value." Assuming this statement to be true, it was shown (3) that the criterion for crack growth in any direction has the general quadratic form

$$a_{11} K_I^2 + a_{12} K_I K_{II} + a_{22} K_{II}^2 = 1 \quad (1)$$

where the constants a_{ij} are functions of the material properties and K_I and K_{II} are the mode I and mode II stress intensity factors.

Wilson (4) has tested slant, center-cracked aluminum plates and has fitted the ellipse of Eq. (1) to the results. The value of K_I increased slightly as K_{II} increased and the intersection of the curve with the K_{II} axis indicated that K_{IIc} , the pure mode II fracture toughness, is probably nearly equal to K_{Ic} , the pure

mode I fracture toughness. Due to the presence of substantial plastic flow around the crack tips in the aluminum, the direction of crack propagation was not in agreement with the hypothesis that a crack moves along a path normal to the direction of greatest tension.

Adhesive joints under combined mode loading have been studied by many investigators. Ripling, et al (5) have studied a lap joint configuration and found the pure mode II fracture toughness to be considerably larger than the pure mode I fracture toughness although the crack did not propagate in a uniform manner. Using a similar specimen geometry, Jemian and Ventrice (6) obtained fracture toughness values and presented evidence, in the form of photoelastic stress patterns, suggesting that crack extension occurs in the opening mode in the lap joint specimens. Knauss (7) has presented a general qualitative description of crack propagation at or near the interface and the parameters, such as the type of loading, which affect crack propagation. Erdogan and Gupta (8, 9) have studied layered systems with flaws in the matrix and at the interface. A stress analysis was performed by solving a system of integral equations. Many combinations of material properties and types of loading were studied. Of particular interest to the present study are the results (8) for two half planes with a modulus of elasticity, E , of 10^7 psi bonded by an adhesive layer ($E = 4.5 \times 10^5$ psi) with a center crack under tensile loading normal to the crack. For an adhesive thickness equal to the crack length, K_{II} increased as the crack moved closer to one of the interfaces. By using the hypothesis that the crack would extend in a direction normal to the maximum tensile stress, they have determined that the direction of crack extension is such that the crack would always tend to propagate away from the interface and towards the center of bond (CoB).

Orthotropic materials under combined mode loading have been studied also. Irwin (10) has suggested that the total strain energy rate, \mathcal{G} , is equal to a constant \mathcal{G}_c ,

$$\mathcal{G} = \mathcal{G}_I + \mathcal{G}_{II} = \mathcal{G}_c \quad (2)$$

For orthotropic materials, a diagram of K_I versus K_{II} with \mathcal{G} constant results in an ellipse with the ratio of the major and minor axes equal to the fourth root of the ratio of the moduli in the principal orthotropic directions. Results by Sanford and Stonesifer (11) from specimens cut from a large diameter, glass fiber wound cylinder substantiate this theory. Wu (12) has reported results on unidirectional glass fiber reinforced epoxy sheets which show that K_I decreased very slowly as K_{II} increased from zero and that the total \mathcal{G} value increased. In a later report Wu (13) analyzed "shear connector fibers" which resulted from crack "skipping". With a stringer force model he showed qualitatively that the constant \mathcal{G} concept could be a fracture criterion under combined mode loads. With the same material, Lauraitis (14) showed good correlation with the constant \mathcal{G} concept by determining the tensile strength for fiber orientations between 0° and 90° and relating this strength to the fracture toughness by assuming the existence of microvoids which extended during loading to a certain critical size.

FINITE ELEMENT ANALYSIS

A homogeneous tension plate with a slant edge crack was analyzed by the finite element method. From the crack line displacements, the mode I and II stress intensity factors (K_I , K_{II}) were calculated and the total strain energy rate, $\dot{\mathcal{U}}$, was determined from the loading line displacements by using the compliance method.

General Procedure

The finite element method was used to determine the displacements necessary to evaluate the required fracture mechanics parameters. The details of the finite element technique have been discussed by many authors (15). A six-node, linear strain triangle was used in this analysis.

The finite element grid pattern for the plate of height, $2H$, width, W , and thickness, B , is shown in Fig. 3. The slant edge crack of length a makes an angle ϕ with the horizontal and is located such that the midpoint of its length is always on the horizontal line which divides the plate into two equal parts. The grid pattern is generated by first locating all the nodes on the boundaries and the first ring of nodes which is 0.003 units from the crack tip. The second ring of nodes is located on the radial lines 0.1 units from the first ring of nodes. The remaining nodes along the radial lines are generated by an arithmetic progression. The nodes are then connected to form quadrilaterals which are, in turn, divided into triangles. The nodes along the upper boundary are loaded by forces which are equivalent to a uniformly, distributed load, P . The vertical displacements of the nodes along the lower boundary are zero and the horizontal displacement of the node in the lower left corner is zero. Since H is 15 units and W is 10 units, these boundary conditions provide a situation very similar to a plate loaded in uniaxial tension.

Three interrelated fracture mechanics parameters are evaluated from the nodal displacements by using the displacement method and the compliance method (1, 16-18). With the displacement method K_I and K_{II} are obtained by evaluating the plane strain crack tip displacement equations along the crack line ($\theta = \pi$):

$$u = \frac{4K_{II}}{E} \sqrt{\frac{r}{2\pi}} (1 - \nu^2) \quad (3)$$

$$v = \frac{4K_I}{E} \sqrt{\frac{r}{2\pi}} (1 - \nu^2) \quad (4)$$

where r is the distance from the crack tip, E is the modulus of elasticity, and ν is Poisson's ratio. The necessary displacements, u for K_{II} and v for K_I , are determined from the nodal displacements as shown in Fig. 4. Consequently, at each pair of crack line nodes the stress intensity factors can be calculated. These calculated values are then plotted versus the relative distance to the crack tip, r/a . As $\frac{r}{a} \rightarrow 0$, the displacement equations become more accurate but the finite element results become less reliable. Consequently, the results are extrapolated to the crack tip ($r = 0$) in order to obtain the desired stress intensity factor. In Fig. 5 this procedure is illustrated for the pure mode I case where $\phi = 0$.

The strain energy rate, \mathcal{G} , is evaluated by the compliance method. The compliance, C , is calculated by dividing the average displacement of the nodes along the upper boundary by the applied load. After evaluating the compliance over a range of crack lengths, the compliance derivative, $\frac{dC}{da}$, which is directly related to \mathcal{G} by the equation

$$\mathcal{G} = \frac{P^2}{2B} \left(\frac{dC}{da} \right) \quad (5)$$

is computed by a moveable strip and least squares curve-fitting technique (19).

General Results

For pure mode I loading, the results of the displacement method are illustrated in the second column of TABLE 1. When these results are compared with the boundary collocation results of Gross, et al (20), the percent difference (difference/average value) is less than 3.3% ($\frac{a}{W} < 0.50$). The results of the compliance method are shown in the last column of TABLE 1. The stress intensity parameter was calculated by using the plane stress relationship

$$K^2 = \mathcal{G} E \quad (6)$$

The percent difference between the compliance results and those of Ref. (20) are less than 1½% except at the shortest and longest relative crack lengths. The larger differences at these crack lengths appear to be due to the inability of the curve fitting technique to accurately fit a curve at the endpoints of the compliance versus crack length results.

For cracks oriented at angles of 15, 30, 45, and 60 degrees, the compliance method was used to calculate the total stress intensity factor parameter, $\frac{KB\sqrt{W}}{P}$ (TABLE 2). With the displacement method the stress intensity factors, K_I and K_{II} , (TABLE 3) were determined and the stress intensity factor parameter,

$$\frac{\left(K_I^2 + K_{II}^2\right)^{\frac{1}{2}} B\sqrt{W}}{P},$$

was calculated. Since (from Eqs. 2 and 6)

$$K^2 = K_I^2 + K_{II}^2 \quad (7)$$

these two stress intensity factor parameters should yield the same value. TABLE 4 shows the percent difference (difference/average) in these two parameters. Percent differences are less than 5.3% except at the shortest and longest relative crack lengths.

Again, some of this can probably be attributed to the inaccuracy of the curve fitting technique at the endpoints.

The results of TABLE 1 and 4 are presented in order to establish confidence in the displacement method of obtaining K_I and K_{II} . In the following section, the results of the finite element displacement method will be presented.

Results of Displacement Method

Using the displacement method, the mode I stress intensity factor parameter,

$$\frac{K_I^2 B^2 W}{P^2},$$

was computed over a range of relative crack lengths at various crack orientations (Fig. 6). Good agreement with the boundary collocation results of Wilson (4) and two additional data points obtained by Smith and Smith (22) by using a photoelastic determination is shown in this figure. In Fig. 7 the mode I stress intensity factor parameter, $\frac{K_I B\sqrt{W}}{P}$, is displayed as a function of crack orientation angle, ϕ , at various relative crack lengths. The influence of the relative crack length on the ratio of the mode I and II stress intensity factors, K_{II}/K_I , is shown in Fig. 8. Again, there is good agreement with the results of Wilson (4) and Smith and Smith (22). These same results are displayed in Fig. 9 where the ratio K_{II}/K_I is plotted versus the crack orientation angle, ϕ . From this figure it can be noted that large ratios of K_{II}/K_I can be obtained with specimens with large crack angles and short crack lengths.

EXPERIMENTAL PROGRAM

Experimental Procedure and Results

The experimental program consisted of testing adhesive joint specimens with single-edge-notched (SEN) slant adhesive layers oriented at various angles, ϕ (Fig. 10). The same specimen preparation that was described in Ref. (1) was used. This procedure involved bonding aluminum adherends with a Dow 332 epoxy resin mixed with 10% TEPA hardener and postcured at 180°F.

Special loading arms were necessary to obtain a sharp, natural precrack in the specimens. The precracking procedure is shown in Fig. 11. A 30X StereoZoom microscope was used to monitor the crack until it had extended a satisfactory depth into the specimen. The specimen was then remounted in the Instron testing machine (Fig. 12) and loaded at a rate of 0.2 in/min until the critical load, P_c , was reached, the crack propagated abruptly, and complete separation occurred. The length of the final precrack was determined from the fracture surface and measured as shown in Fig. 10. For various angles, ϕ , the final crack length, critical load, and \mathcal{G}_I and \mathcal{G}_{II} for crack extension are listed in TABLE 5.

The effect of the location of the crack tip--center-of-bond (CoB) or interface (IF)--is an important consideration. For the pure mode I specimens ($\phi = 0^\circ$), the precrack and the subsequent crack propagation until complete separation was CoB. Most of the combined mode specimens exhibited a general pattern of crack extension where the precrack extended along the upper IF (Fig. 10) until it entered the primary part of the specimen. It then extended to the lower IF probably due to the change in stiffness of the arms where they are attached to the main part of the specimen. After this precracking, the specimen was loaded (Fig. 12) until fast fracture and complete separation occurred. The crack extended rapidly from the lower IF to the upper IF and along the upper IF until complete separation. This

behavior is illustrated on the fracture surfaces of a 45° specimen (Fig. 13).

A magnification of the fracture surface exhibiting fast fracture behavior (region 4 - Fig. 13) is shown in Fig. 14 for another 45° specimen. The fast propagation from one IF to the other occurs approximately perpendicular to the external applied load.

Some differences from the general pattern of crack extension behavior of the combined mode specimens should be emphasized. Figure 15 shows a schematic of the fracture surface of a typical 15° specimen. The CoB crack extension occurred during the initial part of fast fracture in all of the 15° specimens tested. The 15° specimen seems to be in a transition area--the 0° specimens exhibited CoB crack extension and the 30° specimens were IF.

Another difference from the general crack extension pattern occurred in the precracking of two 60° specimens ($a = 1.09, 1.11$ - TABLE 5). Due to the relatively large loads that were necessary to precrack the specimen, the crack extended a large distance into the specimen before it arrested. For these two specimens, the final precrack was CoB. Upon testing the specimen, the crack extended directly to the upper IF and along the upper IF until complete separation.

One 45° specimen ($a = .31$ in., $P_c = 3150$ lb.) was precracked and then cycled from 0 to 2550 lb. as shown in Fig. 16. After 22 cycles the crack jumped from the lower to the upper IF as shown in the photograph of Fig. 16. Upon loading the specimen, the crack propagated along the upper IF until complete separation occurred. The results of this specimen are very close to the average results of all the 45° specimens tested suggesting that the results will be the same for the crack at either IF.

In order to analyze the effects of combined mode loading on the toughness of the adhesive system, the results of the finite element analysis of the slant SEN homogeneous plate were utilized along with the approximation (1) that \mathcal{H} for a one-material (aluminum) system is approximately equal to \mathcal{H} for a two-material

(aluminum-epoxy) system with a very thin adhesive layer. This approach seems appropriate even though the above approximation was analyzed only for a CoB crack under mode I loading. Just as in the pure mode I loading, with pure mode II loading the extreme conditions on the strain energy rate are known. The upper extreme occurs when the adhesive layer is of sufficient thickness such that the strain energy rate of a homogeneous adhesive (epoxy) plate can be used. When the adhesive layer shrinks to zero, the strain energy rate of an aluminum plate can be used as a lower extreme. The variation of the mode II strain energy rate, with adhesive thickness between these two extremes, would no doubt be similar to the variation in the mode I strain energy rate. Hence, the foregoing approximation should be valid for mode II loading or combinations of mode I and mode II loading. The foregoing approximation for \mathcal{G} was also assumed to apply when the crack was located at the IF as well as the CoB. This approximation seems reasonable when one notes that the crack tip was located at both IFs and the CoB in various specimens as discussed previously and yet, all of the results appear to present a consistent pattern.

In Fig. 17 the values of the critical strain energy rates are shown. The scatter is considerable; nevertheless, several important observations can be made. First, the general trend indicates a significant increase in the mode I critical strain energy rate as the mode II strain energy rate increased. This observation would be an important consideration in the design of an adhesively-bonded structure. Secondly, a fracture criteria for the adhesive system that would roughly fit the data would be the general quadratic form given in Eq. 1. The $\mathcal{G}_I + \mathcal{G}_{II} = \mathcal{G}_c$ criteria, which is a straight line between $(\mathcal{G}_I = \mathcal{G}_{Ic}, \mathcal{G}_{II} = 0)$ and $(\mathcal{G}_{II} = \mathcal{G}_{IIc}, \mathcal{G}_I = 0)$, clearly is not appropriate for this adhesive system.

In an early phase of this study of the combined mode crack extension in adhesive systems, slant center-cracked specimens (Fig. 18) with $\phi = 0, 20, 45,$ and 60 degrees were loaded to failure. Cracks of $7/8$ inch length were formed by

embedding a razor blade wrapped in Teflon tape (except for its tip) in the adhesive, and then removing it after gelation. The crack tip provided by the razor blade may be blunted upon removal of the blade from the epoxy. This crack tip may not be sharp enough to insure minimum toughness, although the toughness calculated for the $\phi = 0^\circ$ specimen by using the secant correction for width is very close to the average value calculated from the SEN specimens. Considering the inconsistencies in the crack tip sharpness along with the fact that only one specimen was tested at each orientation angle, only the general trend of the results should be emphasized. To investigate this general trend, the analysis of Sih, Paris, and Erdogan (23) for an infinite, homogeneous tension plate with a slant center crack was used. With Eq. 6 ($K^2 = \mathcal{G} E$) and the approximation that \mathcal{G} for the one-material system is approximately equal to \mathcal{G} for the two-material system for very thin adhesive layers, \mathcal{G}_I and \mathcal{G}_{II} for the two-material system are calculated and shown in parameter form in TABLE 6 along with the results from the center-cracked adhesive specimens. The crack extended from the crack tip formed by the razor blade to the IF and along the IF as shown in Fig. 18. Again, the general trend of the results shows an increase in the mode I critical strain energy rate as the mode II critical strain energy rate increases.

Discussion of Results

In the experimental program adhesive joint specimens with precracked SEN slant adhesive layers were loaded until crack extension occurred. The observed CoB crack extension for pure mode I loading ($\phi = 0^\circ$) is consistent with the concepts of Ref. 8. In that paper an increasing value of K_{II} was noted (pure mode I loading) as the crack moved closer to the IF. With the hypothesis that the crack would extend normal to the maximum tensile stress, it was shown that the crack extension would thus be CoB.

With the SEN specimens ($\phi = 0^\circ$) used in this study, there would undoubtedly be an increase in the K_{II} value as the crack moved closer to the IF. With this increase, the value of K_I for crack extension would increase which would, in turn, tend to drive the crack to the CoB.

Cracks in the adhesive layer of the combined mode specimens moved along a path normal to the applied load except when the crack reached the adherend (aluminum) it extended along the IF. The CoB-IF crack extension observed in the 15° specimens is an exception. This behavior seems to be due to a balance of conflicting tendencies, first the CoB tendency noted previously for the 0° specimens and second, the tendency for the crack to extend in a direction normal to the applied load. The CoB precracking behavior observed in two of the 60° specimens can be described in a similar manner. The first segment of precracking was greatly influenced by the high precracking load which initially drove the crack to the IF. As the load dropped off and the crack decelerated during precracking, the CoB influence became predominant, and the crack extended to the CoB.

SUMMARY AND CONCLUSIONS

The problem of combined mode crack extension in a SEN specimen with a slant adhesive layer was investigated. A finite element analysis was used to obtain the mode I strain energy rate, \mathcal{G}_I , and the mode II strain energy rate, \mathcal{G}_{II} , for a homogeneous tension plate with a slant SEN. By utilizing the crack extension results from aluminum-epoxy-aluminum specimens along with the approximation (1) that for a very thin adhesive layer \mathcal{G} for the two-material system is approximately equal to \mathcal{G} for the one-material system, the interaction of \mathcal{G}_I and \mathcal{G}_{II} at crack extension was obtained.

The finite element method was applied to a homogeneous tension plate with a slant SEN where a radial array of elements with a small hole at the crack tip served as an adequate grid system. The finite element displacement method provided both K_I and K_{II} . The total K obtained by the finite element compliance method compared well with $(K_I^2 + K_{II}^2)^{\frac{1}{2}}$, particularly for the middle range of crack lengths. At the shortest and longest crack lengths, inaccuracies were probably due to the curve fitting technique used to obtain K . The displacement method results agree well with Wilson's results (4).

An important conclusion can be drawn from the general trend of the results shown in Fig. 17--the mode I strain energy rate for crack extension increases significantly as the mode II strain energy rate for crack extension increases. All of the results have this same general trend, although the crack tip was located at both IFs and the CoB in various specimens. Further, these results show that the $\mathcal{G}_I + \mathcal{G}_{II} = \mathcal{G}_c$ failure criteria is not appropriate for the adhesive system but that the general quadratic form (Eq. 1) could be fitted to the data.

REFERENCES

1. G. G. Trantina, "Part One: Fracture Mechanics Approach to Adhesive Joints," Ph. D. Thesis, Theoretical and Applied Mechanics Department, University of Illinois, 1971, also T. & A. M. Report No. 350, August 1971.
2. G. R. Irwin, "Analysis of Stresses and Strains Near the End of a Crack Traversing a Plate," Journal of Applied Mechanics, Transactions of the ASME, 1957, pp. 361-364.
3. F. Erdogan and G. C. Sih, "On the Crack Extension in Plates Under Plane Loading and Transverse Shear," Journal of Basic Engineering, Transactions of the ASME, 1963, pp. 519-527.
4. W. K. Wilson, "On Combined Mode Fracture Mechanics," Ph. D. Thesis, Mechanical Engineering Department, University of Pittsburgh, 1969, also Westinghouse Research Report 69-1E7-FMECH-R1.
5. E. J. Ripling, S. Mostovoy and R. L. Patrick, "Application of Fracture Mechanics to Adhesive Joints," ASTM STP No. 360, Symposium on Recent Developments in Adhesion Science, 1963.
6. W. A. Jemian and M. B. Ventrice, "The Fracture Toughness of Adhesive-Bonded Joints," Journal of Adhesion, Vol. 1, July 1969, pp. 190-207.
7. W. G. Knauss, "Fracture Mechanics and the Time Dependent Strength of Adhesive Joints," Journal of Composite Materials, Vol. 5, April 1971, pp. 176-192.
8. F. Erdogan and G. Gupta, "The Stress Analysis of Multi-Layered Composites with a Flaw," International Journal of Solids and Structures, Vol. 7, 1971, pp. 39-61.
9. F. Erdogan and G. Gupta, "Layered Composites with an Interface Flaw," International Journal of Solids and Structures, Vol. 7, 1971, pp. 1089-1107.
10. G. R. Irwin, "Fracture Mechanics Applied to Adhesive Systems," Patrick, R. L., Treatise on Adhesion and Adhesives, Marcel Dekker, Inc., New York, 1967, pp. 233-267.
11. R. J. Sanford and F. R. Stonesifer, "Fracture Toughness Measurements in Unidirectional Glass-Reinforced-Plastics," Journal of Composite Materials, Vol. 5, April 1971, pp. 241-245.
12. E. M. Wu and R. C. Reuter, "Crack Extension in Fiberglass Reinforced Plastics," University of Illinois, T. & A. M. Report No. 275, 1965.
13. E. M. Wu, "Discontinuous Mode of Crack Extension in Unidirectional Composites," University of Illinois, T. & A. M. Report No. 309, 1968.

14. K. Lauraitis, "Tensile Strength of Off-Axis Unidirectional Composites," University of Illinois, T. & A. M. Report No. 344, August 1971.
15. O. C. Zienkiewicz, The Finite Element Method in Structural and Continuum Mechanics, McGraw-Hill, 1967.
16. S. K. Chan, I. S. Tuba and W. K. Wilson, "On the Finite Element Method in Linear Fracture Mechanics," Engineering Fracture Mechanics, Vol. 2, 1970, pp. 1-17.
17. A. S. Kobayashi, D. E. Maiden, B. J. Simon and S. Iida, "Application of Finite Element Analysis Method to Two-Dimensional Problems in Fracture Mechanics," ASME Paper No. 69-WA/PVP-12, 1969.
18. G. P. Anderson, V. L. Ruggles, and G. S. Stibor, "Use of Finite Element Computer Programs in Fracture Mechanics," International Journal of Fracture Mechanics, Vol. 7, No. 1, March 1971, pp. 63-76.
19. J. P. Gallagher, "Experimentally Determined Stress Intensity Factors for Several Contoured Double Cantilever Beam Specimens," presented at the Second National Symposium on Fracture Mechanics, June 1968.
20. E. Gross, J. E. Srawley and W. F. Brown, "Stress-Intensity Factors for a Single-Edge-Notch Tension Specimen by Boundary Collocation of a Stress Function," NASA TN D-2395, 1964.
21. W. W. Gerberich and Y. Katz, "On a Trigonometric Expression for the Single-Edge-Notch Specimen," Engineering Fracture Mechanics, Vol. 1, 1969, pp. 569-570.
22. D. G. Smith and C. W. Smith, "Photoelastic Determination of Mixed Mode Stress Intensity Factors," presented at the Fourth National Symposium on Fracture Mechanics, August 24-26, 1970, Carnegie-Mellon University, Pittsburgh, Pennsylvania.
23. G. C. Sih, P. C. Paris, F. Erdogan, "Crack-Tip, Stress Intensity Factors for Plane Extension and Plate Bending Problems," Journal of Applied Mechanics, Transactions of the ASME, 1962, pp. 306-312.

TABLE 1

COMPARISON OF METHODS OF DETERMINATION OF THE PURE
MODE I ($\phi = 0^\circ$) STRESS INTENSITY PARAMETER, $\frac{K_I B\sqrt{W}}{P}$

Relative Crack Length $\frac{a}{W}$	Displacement Method $\frac{K_I B\sqrt{W}}{P}$	Percent Difference Between \longleftrightarrow	Ref. (20) $\frac{K_I B\sqrt{W}}{P}$	Percent Difference Between \longleftrightarrow	Compliance Method $\frac{K_I B\sqrt{W}}{P}$
.07	0.54	0.0	0.54	- 9.6	0.49
.11	0.72	+2.8	0.70	- 1.4	0.69
.16	0.94	+3.3	0.91	- 1.1	0.90
.22	1.20	+1.7	1.18	0.0	1.18
.29	1.57	+0.6	1.56	+0.6	1.57
.37	2.11	+0.5	2.10	+1.4	2.13
.46	2.97	-1.0	3.00	- 0.3	2.99
.56	4.38	-4.5	*4.58	- 1.1	4.53
.67	7.22	-9.1	*7.91	-10.9	7.09

*Ref. (21)

TABLE 2

TOTAL STRESS INTENSITY PARAMETER, $\frac{KB\sqrt{W}}{P}$,
DETERMINED BY COMPLIANCE METHOD

Relative Crack Length $\frac{a}{W}$	$\frac{KB\sqrt{W}}{P}$			
	$\phi = 15^\circ$	$\phi = 30^\circ$	$\phi = 45^\circ$	$\phi = 60^\circ$
.07	.38	.36	.33	.25
.11	.66	.58	.47	.33
.16	.88	.77	.61	.42
.22	1.14	.98	.75	.50
.29	1.46	1.24	.93	.61
.37	1.95	1.60	1.17	.73
.46	2.79	2.18	1.50	.89
.56	4.19	3.11	1.96	1.08
.67	5.99	4.24	2.50	1.25

TABLE 3

MODE I AND II STRESS INTENSITY PARAMETERS
DETERMINED BY DISPLACEMENT METHOD

Relative Crack Length $\frac{a}{W}$	$\frac{K_I B\sqrt{W}}{P}$			
	$\phi = 15^\circ$	$\phi = 30^\circ$	$\phi = 45^\circ$	$\phi = 60^\circ$
.07	.50	.40	.26	.13
.11	.67	.55	.38	.20
.16	.88	.72	.50	.28
.22	1.12	.93	.64	.35
.29	1.47	1.19	.82	.44
.37	1.97	1.56	1.05	.56
.46	2.73	2.12	1.35	.69
.56	4.04	3.00	1.80	.86
.67	6.50	4.57	2.47	1.07
	$\frac{K_{II} B\sqrt{W}}{P}$			
	$\phi = 15^\circ$	$\phi = 30^\circ$	$\phi = 45^\circ$	$\phi = 60^\circ$
.07	.13	.21	.23	.20
.11	.14	.24	.27	.24
.16	.16	.27	.31	.28
.22	.19	.32	.37	.33
.29	.24	.40	.44	.40
.37	.32	.51	.53	.47
.46	.39	.66	.66	.55
.56	.47	.87	.83	.65
.67	.73	1.14	1.07	.80

TABLE 4

COMPARISON OF COMPLIANCE METHOD

$$\left(\frac{KB\sqrt{W}}{P} \right) \text{ AND DISPLACEMENT METHOD } \left(\frac{(K_I^2 + K_{II}^2)^{\frac{1}{2}} B\sqrt{W}}{P} \right)$$

Relative Crack Length $\frac{a}{W}$	Percent Difference				
	$\phi = 0^\circ$	$\phi = 15^\circ$	$\phi = 30^\circ$	$\phi = 45^\circ$	$\phi = 60^\circ$
.07	-9.7	-31.8	-22.8	-8.3	+2.5
.11	-4.2	-3.9	-3.1	+0.2	+4.9
.16	-4.3	-1.9	-0.1	+2.5	+5.2
.22	-1.7	-0.3	-0.6	+1.7	+5.3
.29	0.0	-2.0	-1.6	-0.4	+1.3
.37	+0.9	-2.0	-2.5	0.0	+0.3
.46	+0.7	+1.1	-1.8	0.0	+1.2
.56	+3.4	+2.9	-0.6	-1.1	+0.3
.67	-1.8	-8.8	-10.5	-7.7	-6.3

TABLE 5

CRACK EXTENSION RESULTS FOR SEN ADHESIVE BOND SPECIMENS

ϕ	a	P _c	\mathcal{U}_I	\mathcal{U}_{II}
0°	.12	2680	.34	0
	.16	2100	.30	0
	.18	2100	.35	0
	.20	1900	.33	0
	.25	1620	.33	0
	.25	1620	.33	0
	.28	1460	.31	0
	.32	1340	.32	0
15°	.22	1900	.32	.01
	.24	2140	.47	.02
	.27	2130	.55	.02
30°	.20	3500	.65	.13
	.23	3360	.72	.13
	.31	2500	.61	.09
45°	.20	3700	.35	.19
	.31	3150	.48	.19
	.31	2730	.36	.14
	.37	2800	.50	.18
	.38	3130	.65	.23
	.39	3060	.64	.22
	.40	2850	.59	.20
	.45	2900	.73	.23
	.50	2400	.60	.18
60°	.61	3520	.53	.41
	1.09	1750	.41	.25
	1.11	2380	.79	.48

TABLE 6

CRACK EXTENSION RESULTS FOR CENTER-NOTCHED
ADHESIVE SPECIMENS (FIGURE 18)

$$\frac{\mathcal{G}_I E}{\pi a} = \sigma^2 \cos^4 \phi$$

$$\frac{\mathcal{G}_{II} E}{\pi a} = \sigma^2 \sin^2 \phi \cos^2 \phi$$

$$a = \frac{7}{16} \text{ in.}$$

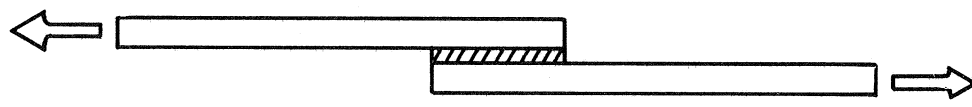
$$W = 2 \text{ in.}$$

$$\sigma = \text{remote stress}$$

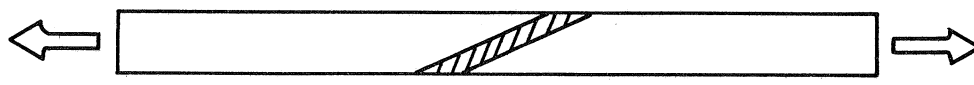
ϕ	σ , ksi	$\frac{\mathcal{G}_I E}{\pi a}$, (ksi) ²	$\frac{\mathcal{G}_{II} E}{\pi a}$, (ksi) ²
0°	1.32	1.74	0
20°	1.82	2.56	0.35
45°	3.60	3.24	3.24
60°	7.35	3.38	10.11



Butt

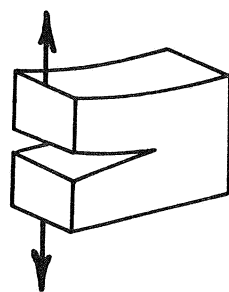


Lap

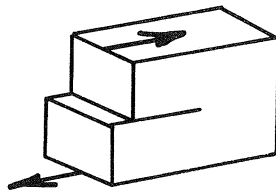


Scarf

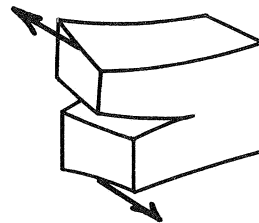
Fig. I Common Types of Adhesive Joints



Mode I



Mode II



Mode III

Fig. 2 Modes of Crack Surface Displacements

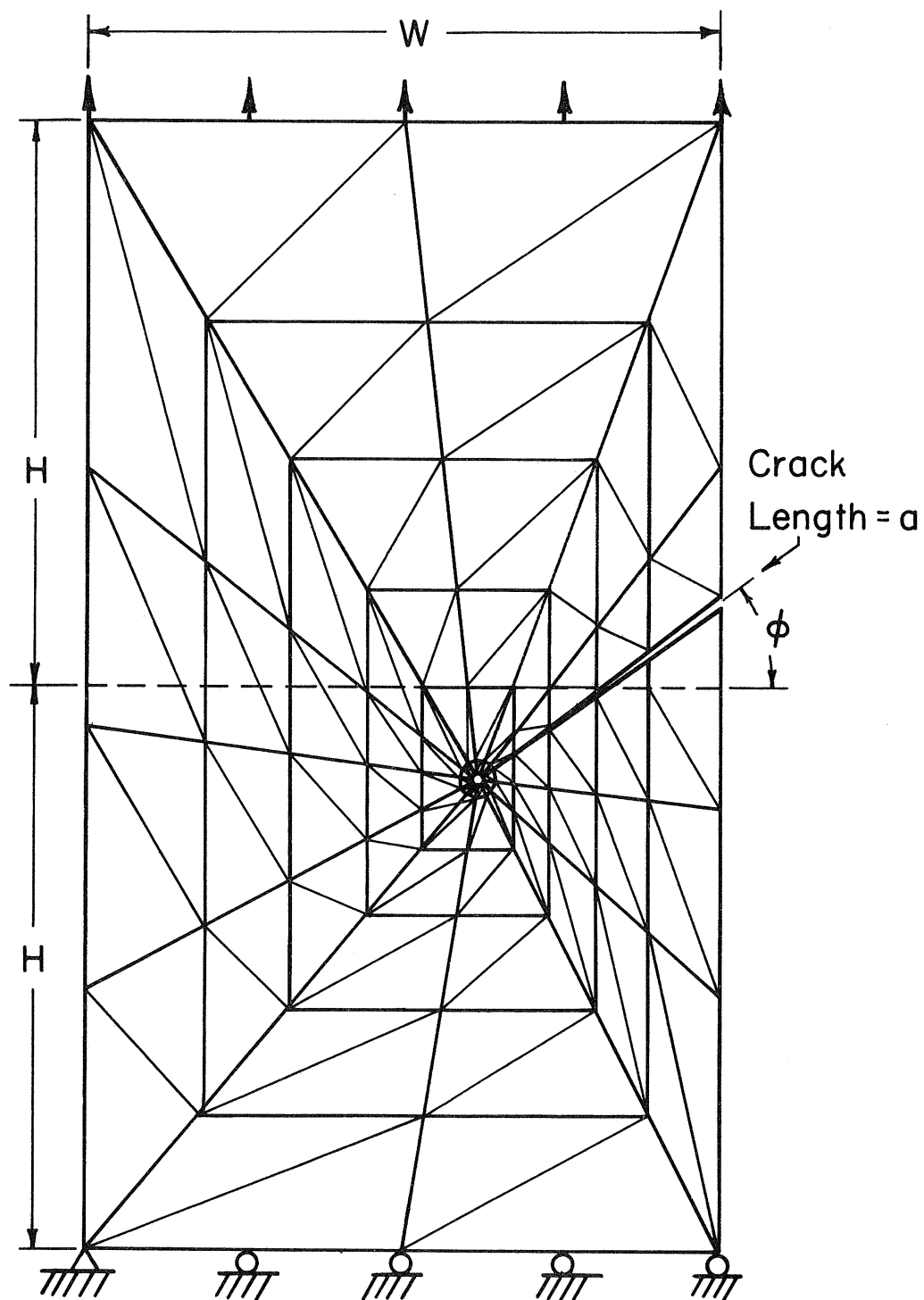


Fig.3 Finite Element Grid Pattern (Not to Scale)

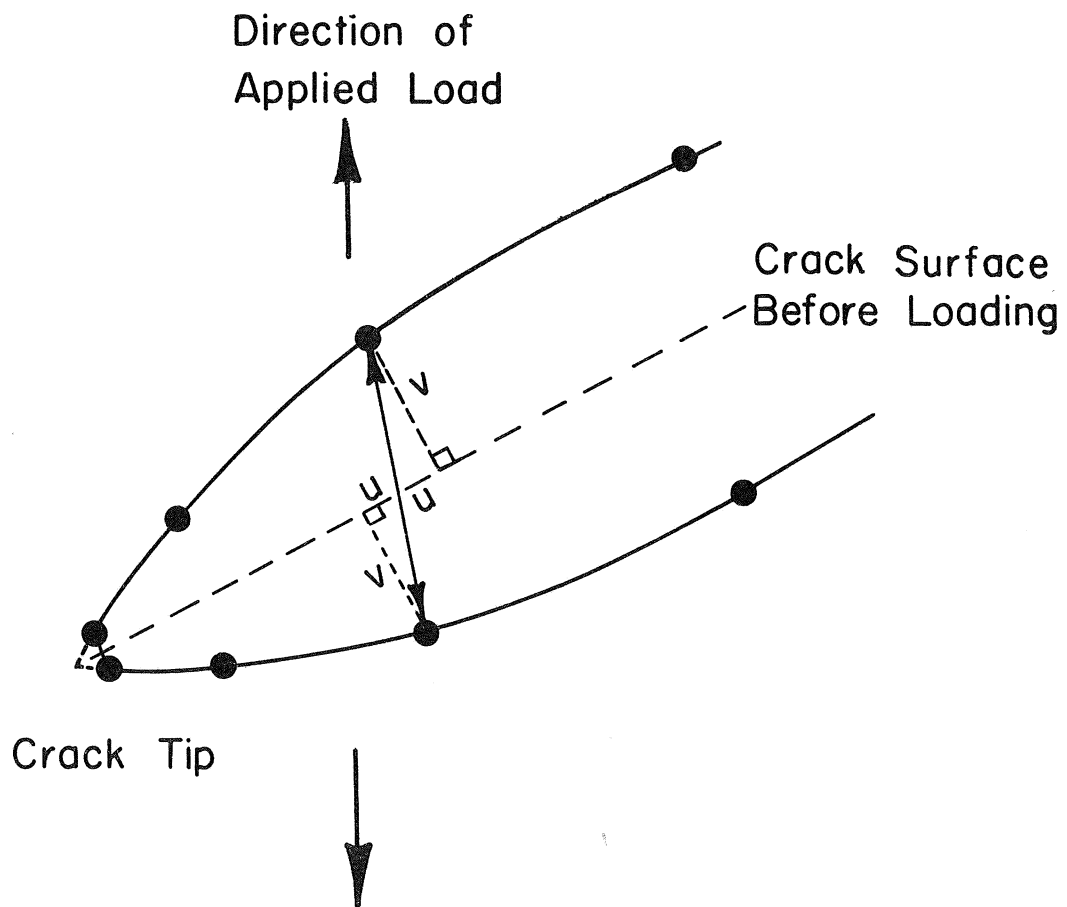


Fig. 4 Crack Surface Displacements in
Vicinity of Crack Tip

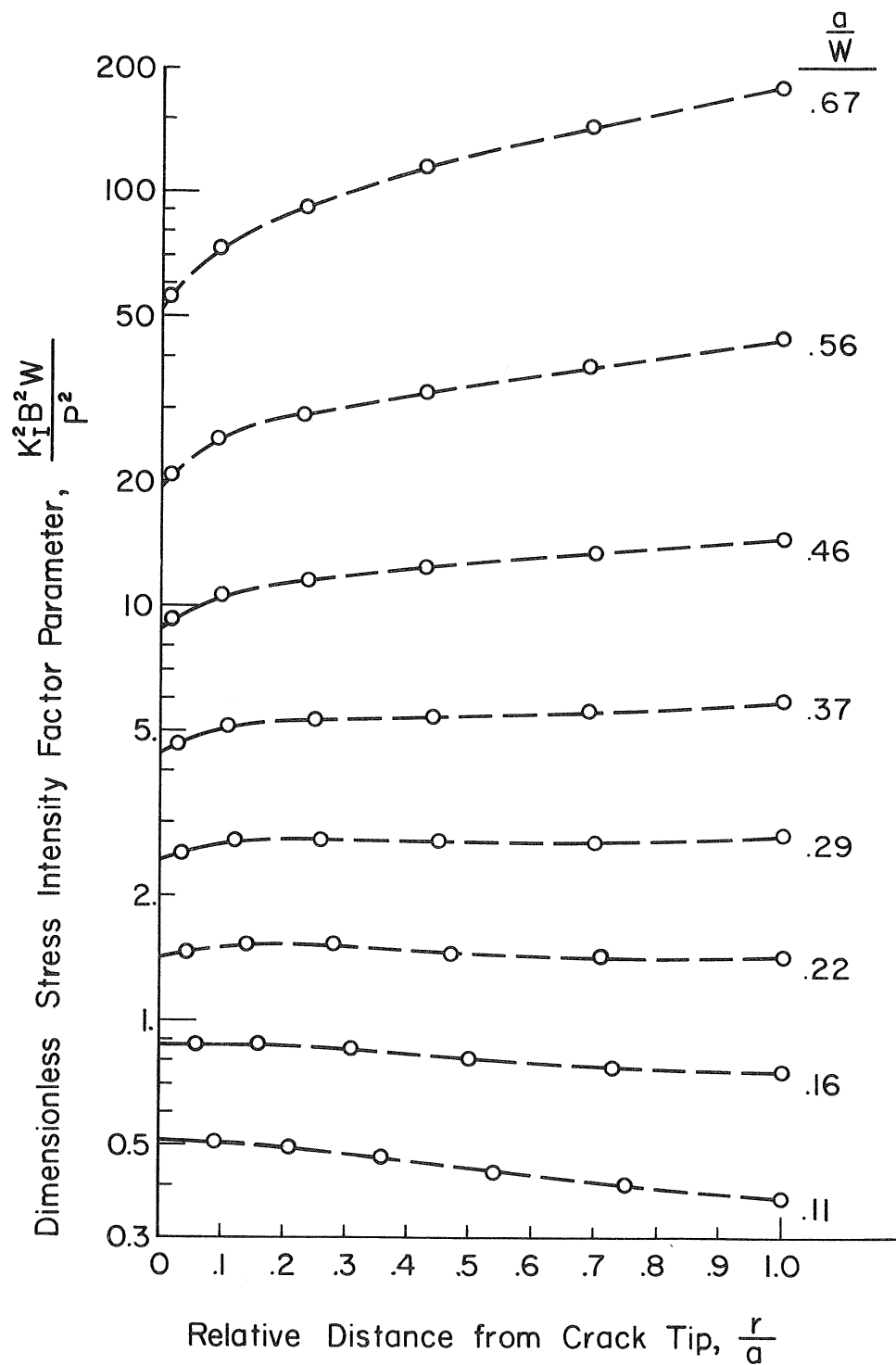


Fig. 5 Displacement Method Extrapolation
 Procedure to obtain Stress Intensity Factors
 ($\phi = 0^\circ$)

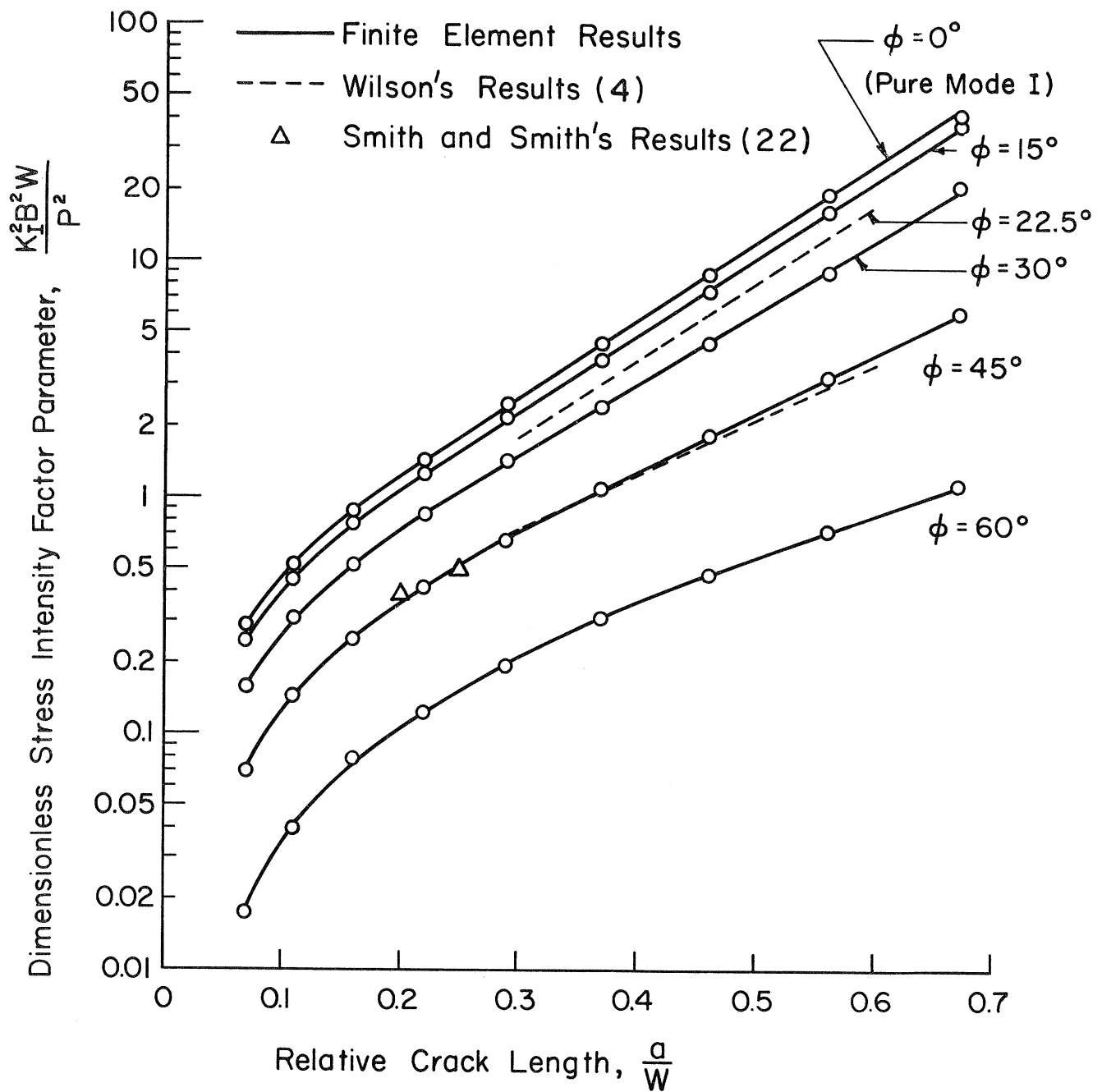


Fig. 6 Mode I Stress Intensity Factors as a Function of Crack Length at Various Crack Orientations

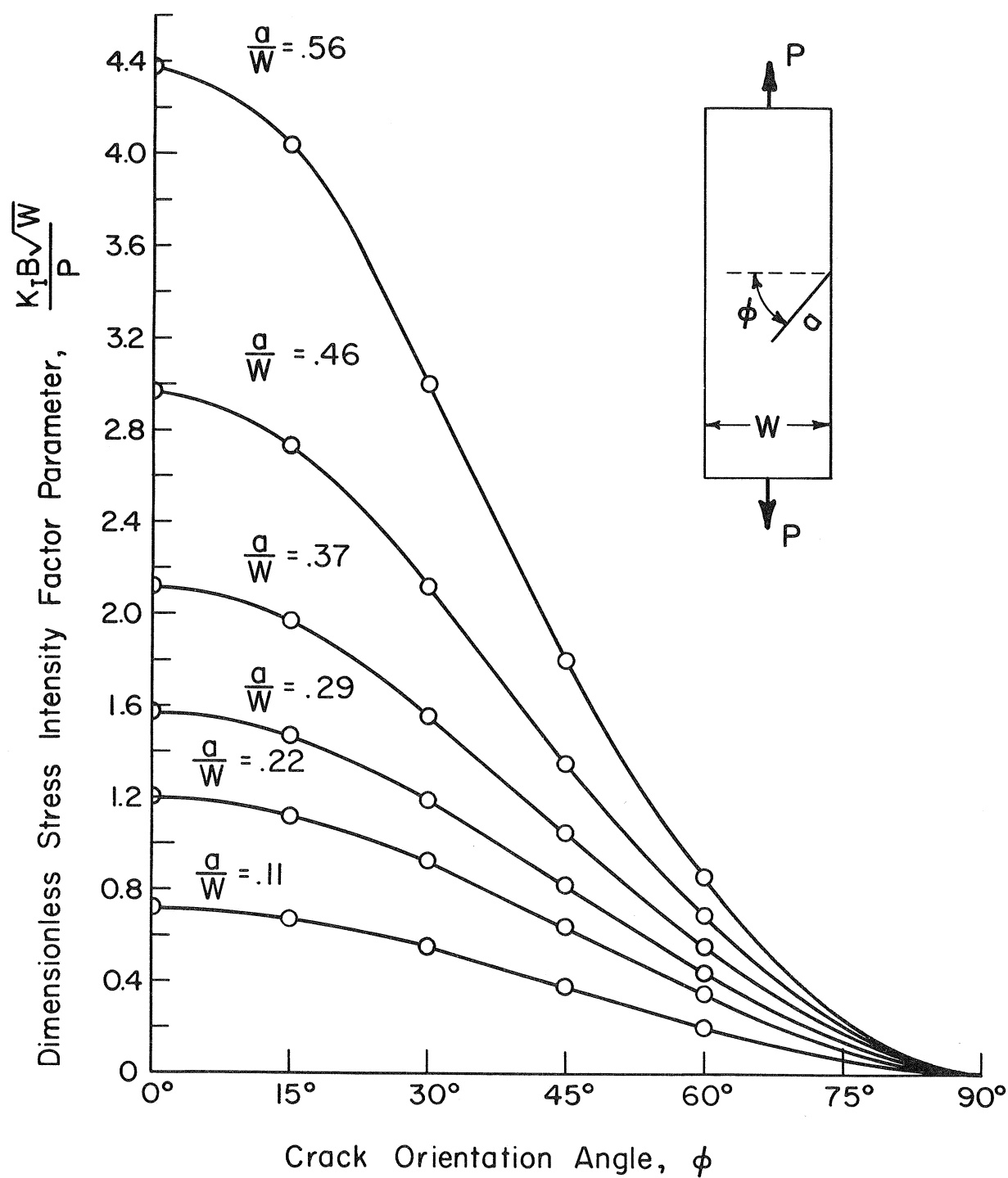


Fig. 7 Mode I Stress Intensity Factors as a Function of Crack Orientation Angle at Various Crack Lengths

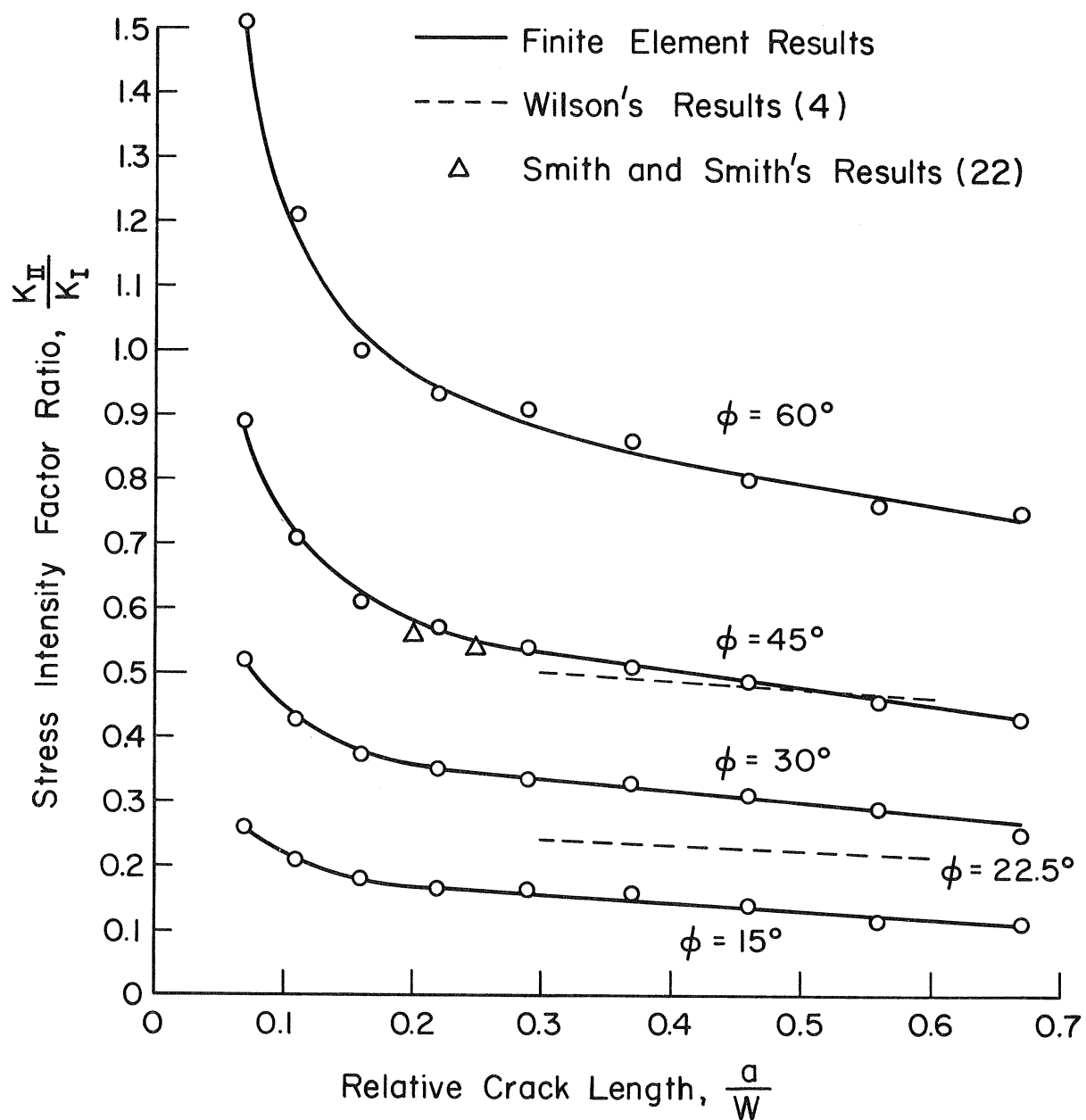


Fig. 8 Stress Intensity Factor Ratio as a Function of Crack Length at Various Crack Orientations

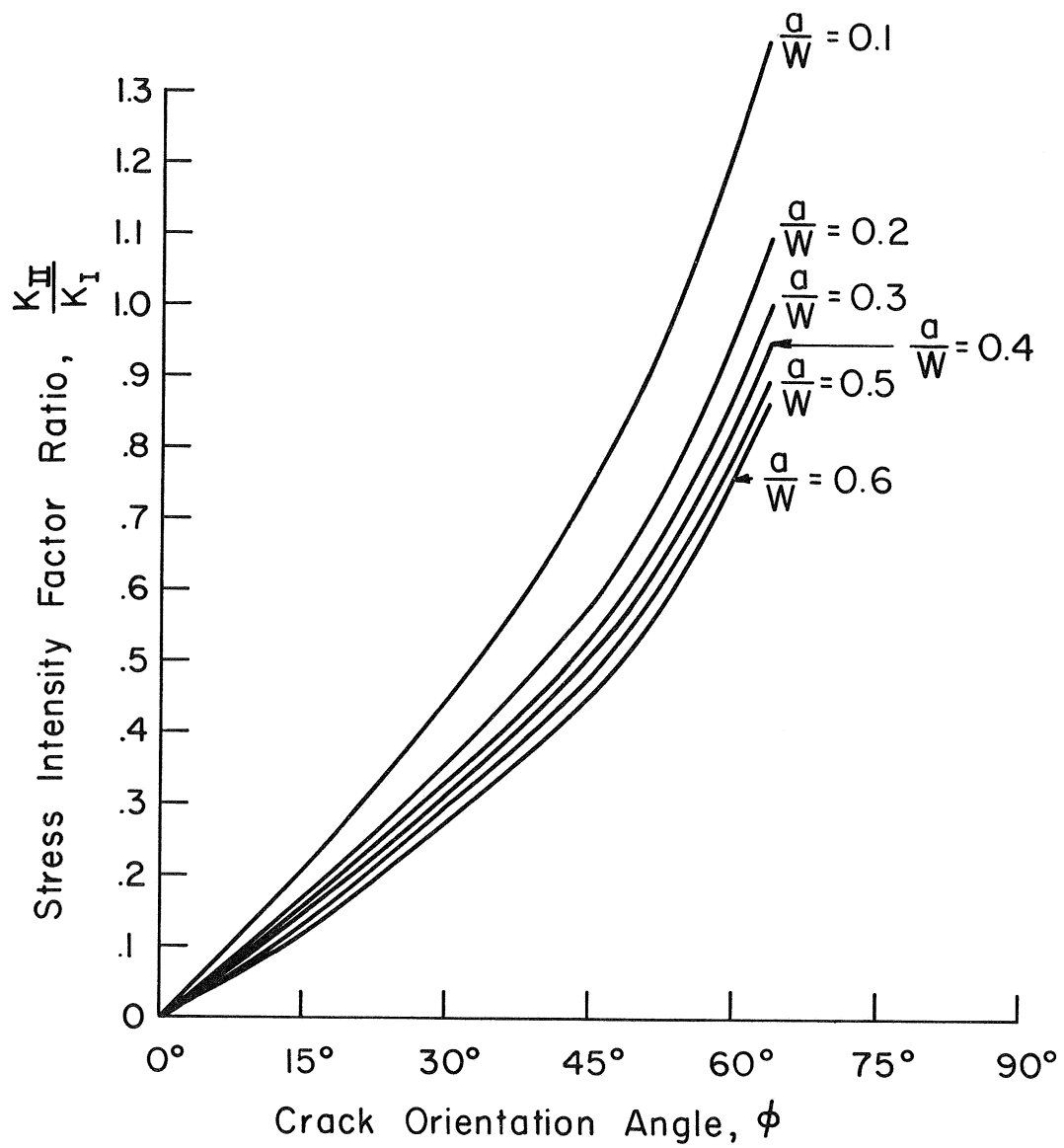


Fig. 9 Stress Intensity Factor Ratio versus Crack Orientation Angle at Various Crack Lengths

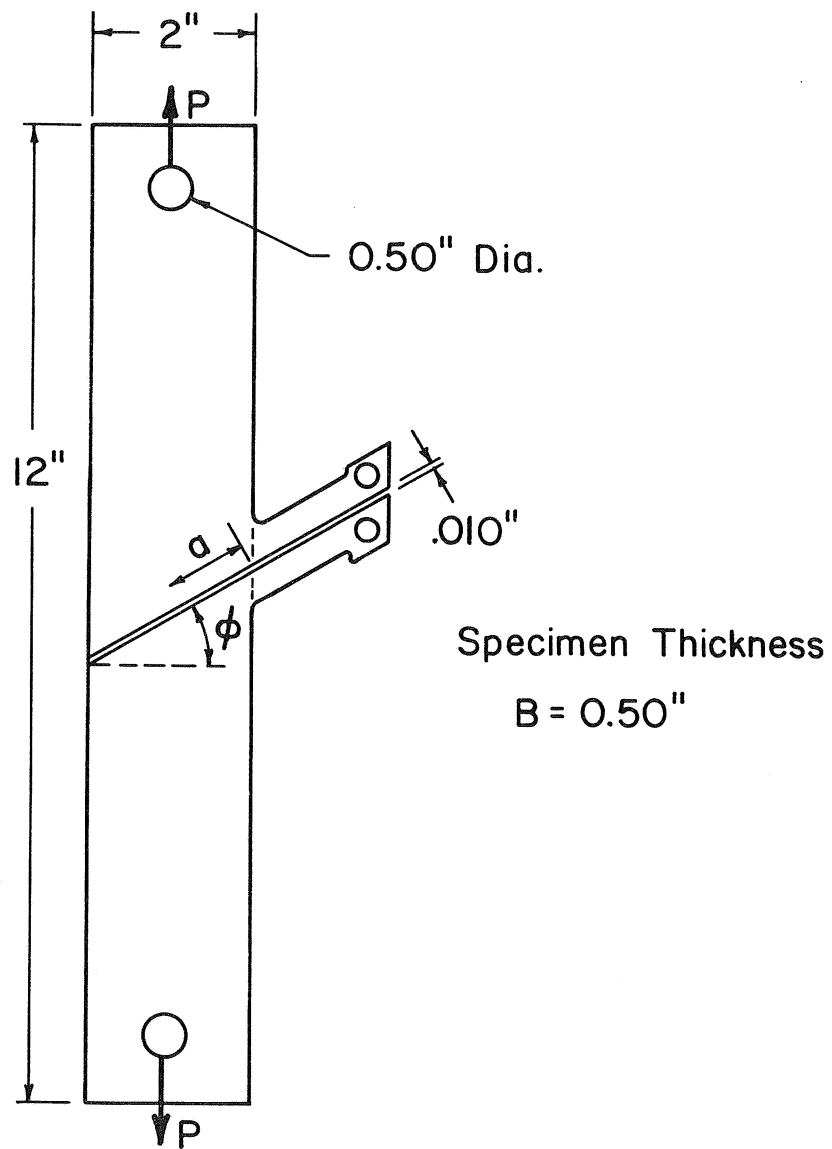


Fig. 10 SEN Combined Mode Specimen

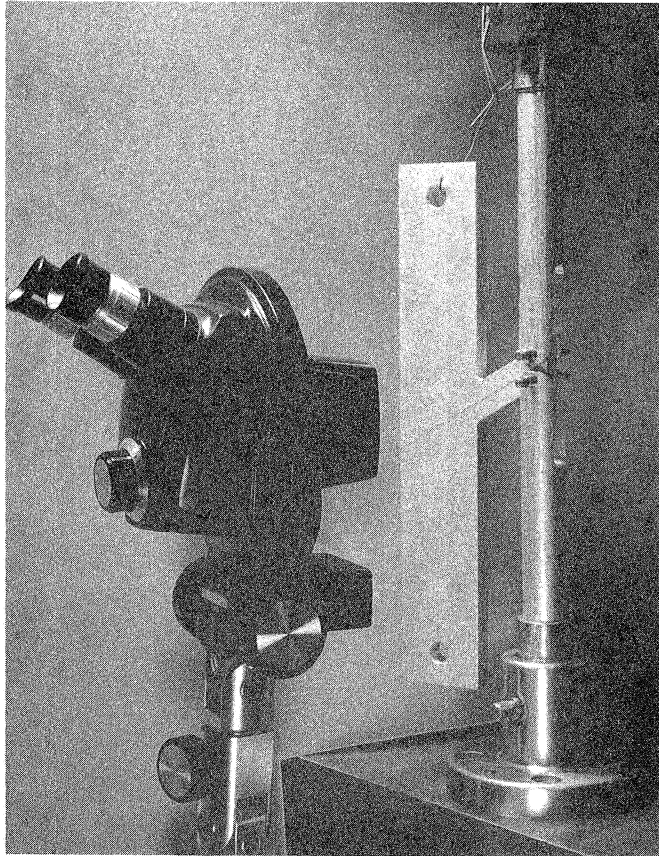


Fig.II Precracking of Specimen

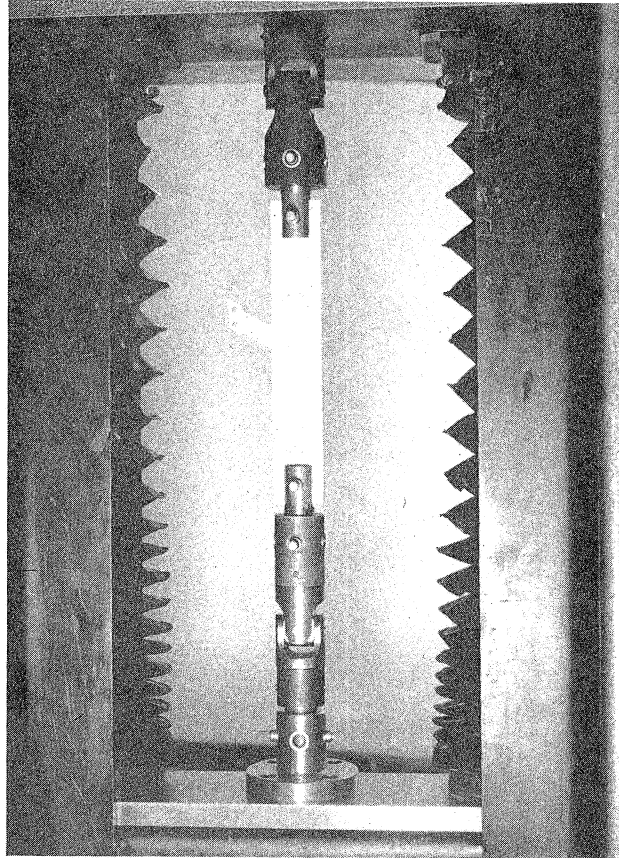
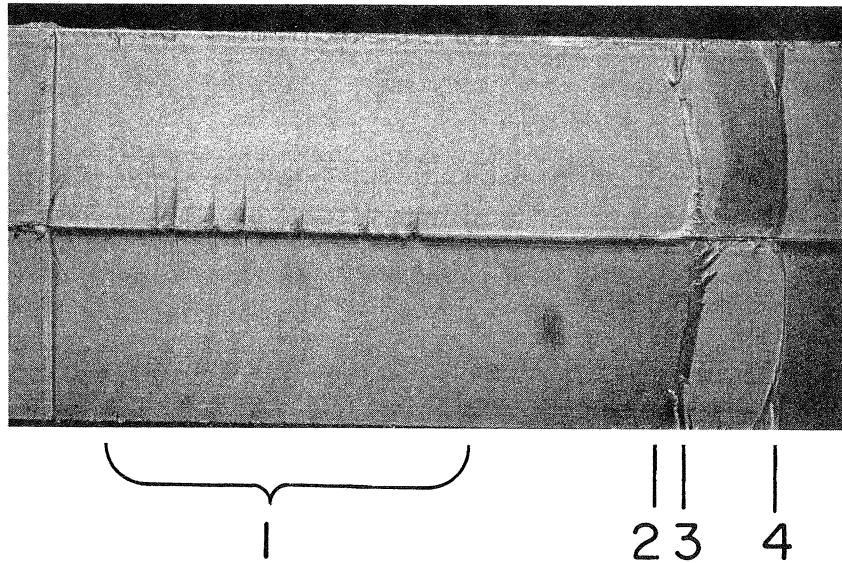


Fig.12 Fracture Testing of Specimen



1. Crack Arrest Markings During Precracking (CoB)
2. Crack Enters Main Part of Specimen
3. Change from CoB to IF
4. Change from Lower IF to Upper IF Upon Fast Fracture

Fig. 13 Fracture Surfaces of 45° Specimen

Direction of Crack Propagation

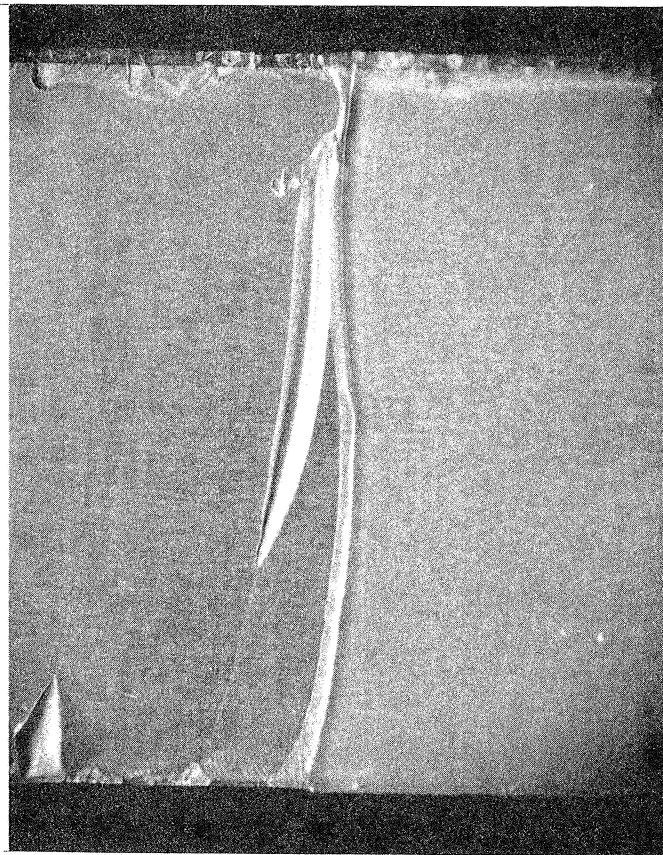


Fig. 14 Fracture Surface of 45° Specimen
Exhibiting Fast Fracture Behavior

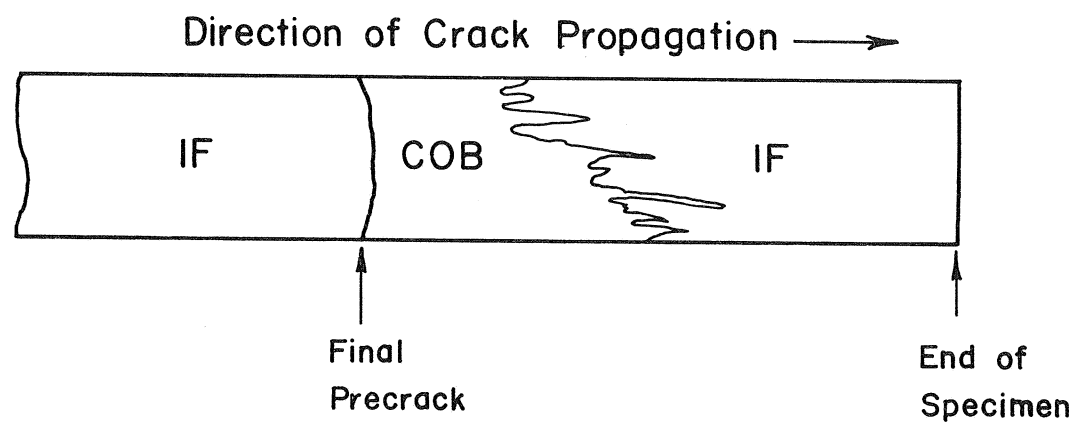


Fig.15 Schematic of Fracture Surface of 15° Specimen

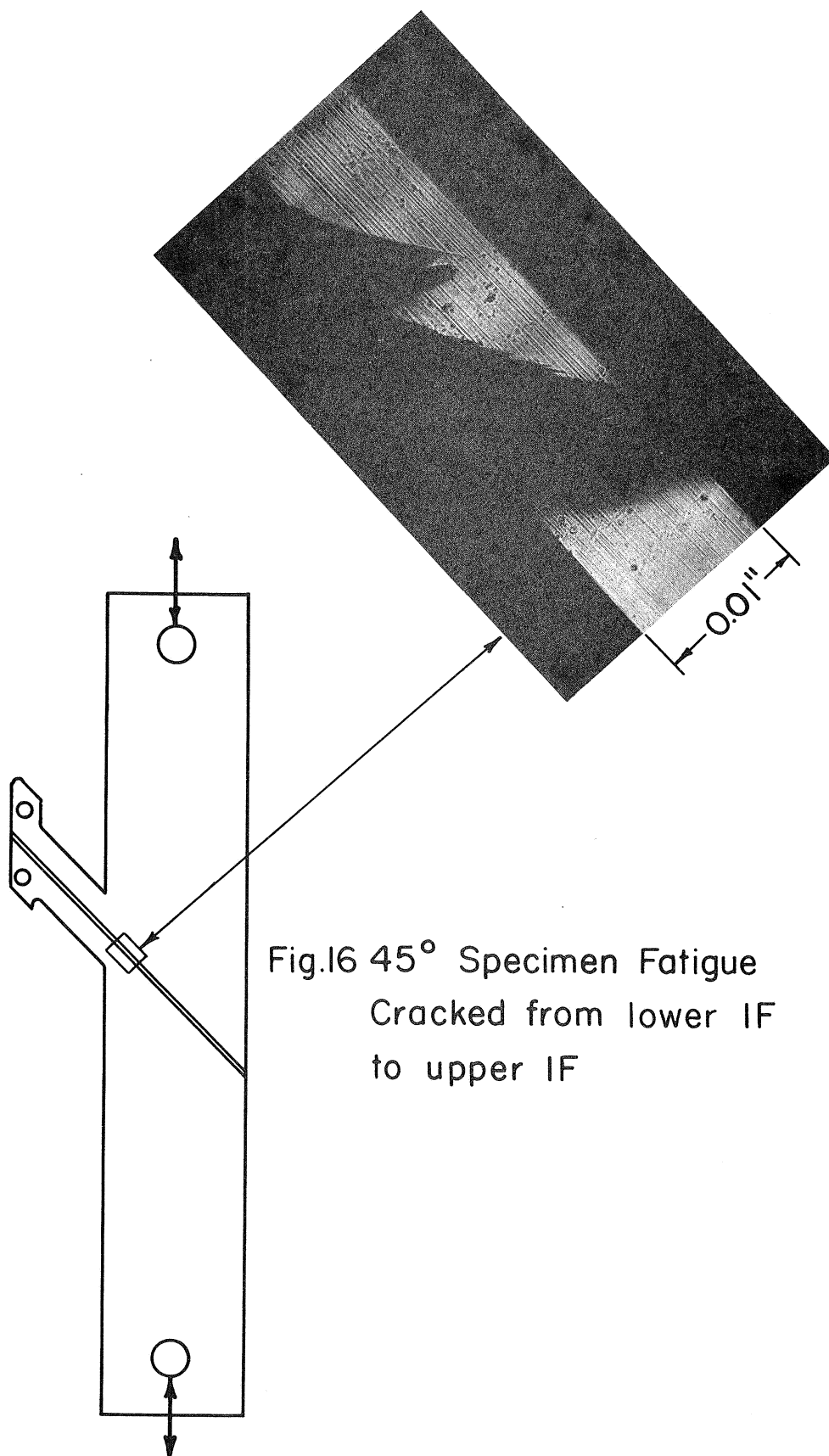


Fig.16 45° Specimen Fatigue
Cracked from lower IF
to upper IF

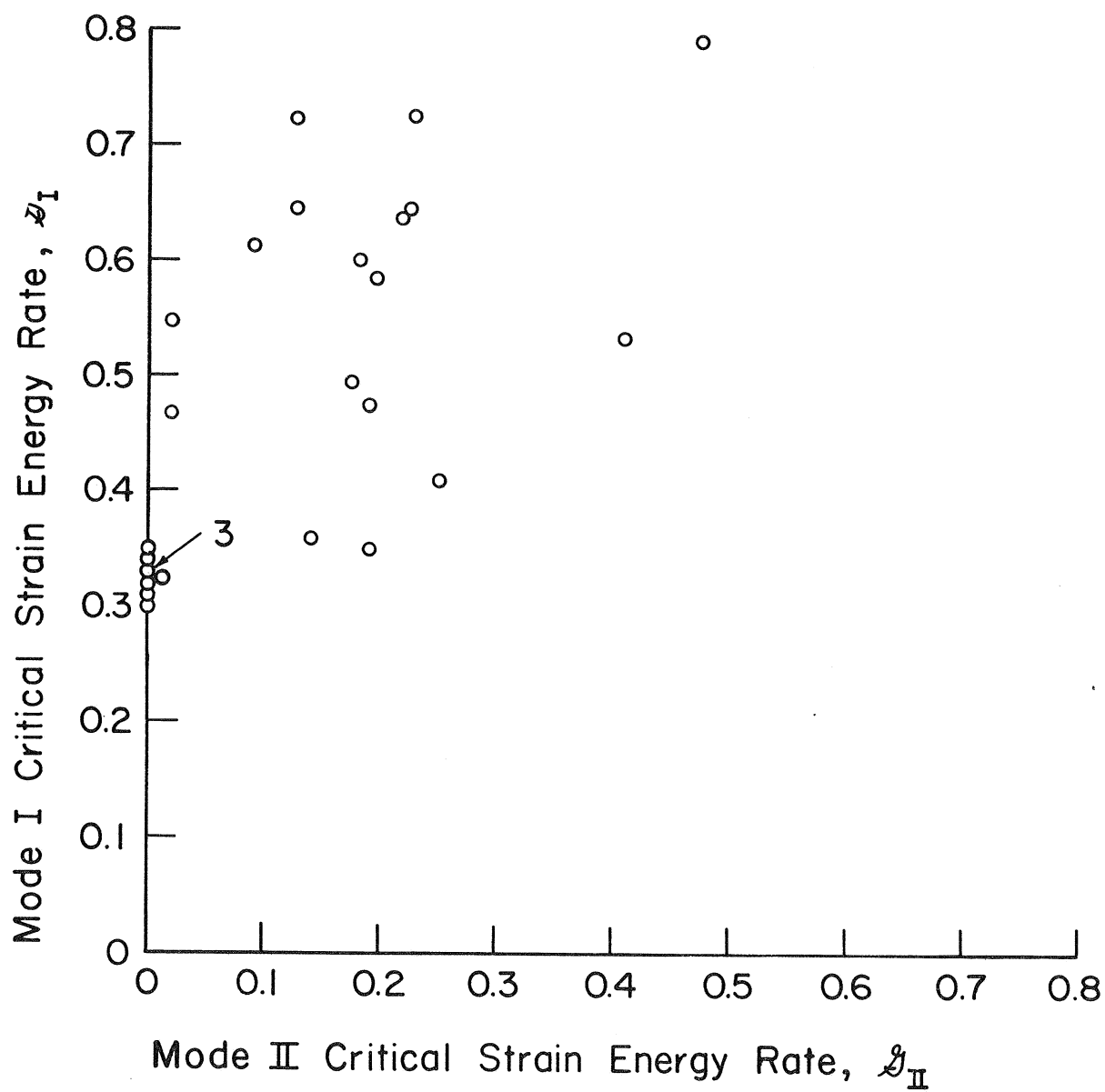


Fig. 17 Interaction Between \mathscr{G}_I and \mathscr{G}_{II} at Crack Extension

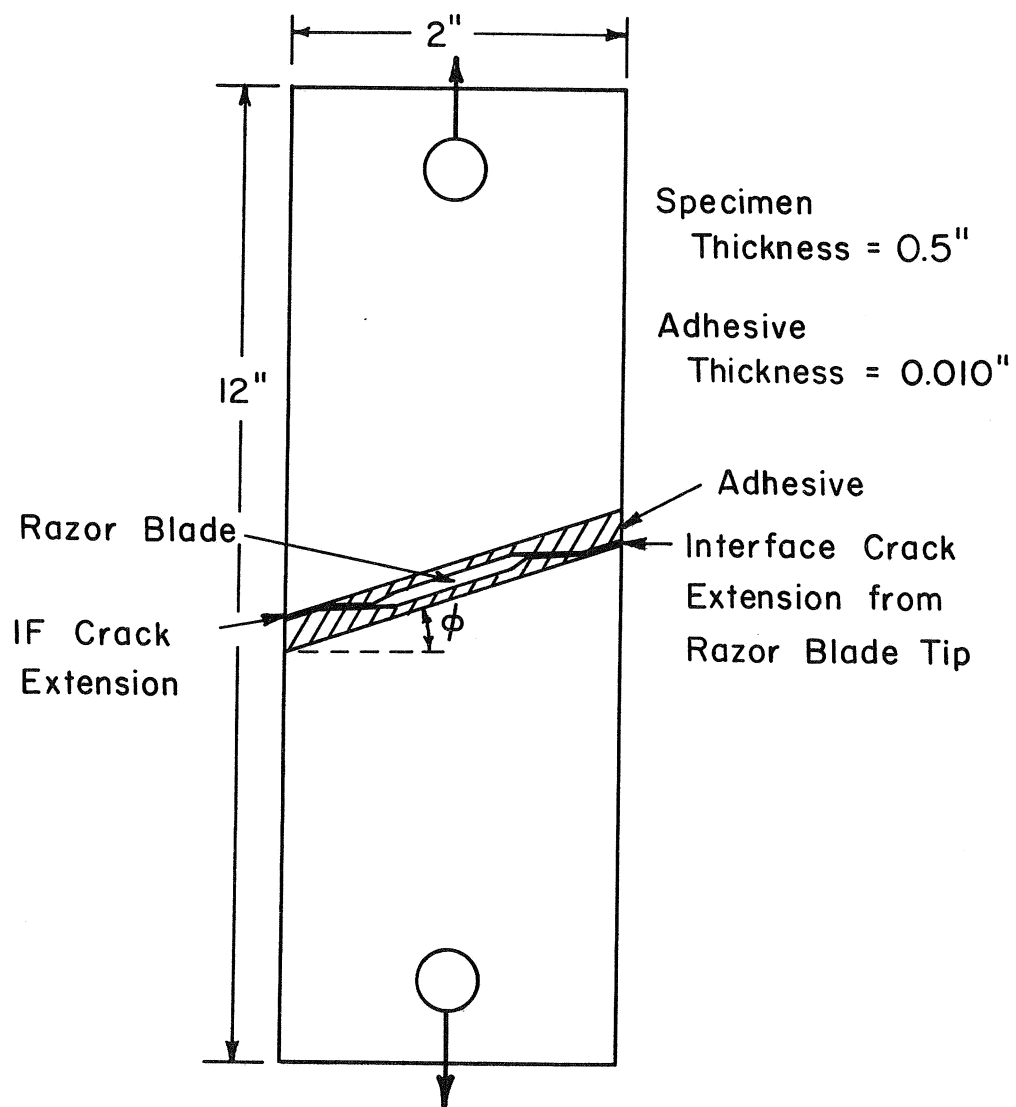


Fig. 18 Center - Notched Adhesive Specimen For Studying Combined Mode Crack Extension (Not to Scale)

Distribution List for Contract N000 19-71-C-0323

with Department of Theoretical and Applied Mechanics, University of Illinois

	<u>No. of Copies</u>
1. AIR -52032A Naval Air Systems Command Washington, D. C. 20360	5
2. Naval Research Laboratory Washington, D. C. 20390 Code 6100 1 Copy Code 6120 1 Copy Code 8430 1 Copy Code 8433 1 Copy	4
3. Naval Ordnance Laboratory White Oak, Maryland 20910 Attention: Code 234	1
4. Naval Ship Engineering Center Washington, D. C. 20360 Attention: Code 6101E	1
5. Naval Ship R. & D. Center Anapolis, Maryland	1
6. Naval Ship R. & D. Center Washington, D. C. 20007 Attention: Code 725	1
7. Chief of Naval Research Washington, D. C. 20360	1
8. Materials Research Laboratory, Inc. One Science Road Glenwood, Illinois 60425	1
9. Alpha R. & D. Inc. 14323 So. Western Avenue Blue Island, Illinois 60406	1
10. ORD-0333A Naval Ordnance Systems Command Washington, D. C. 20360	1

Distribution List for Contract N000 19-71-C-0323

with Department of Theoretical and Applied Mechanics, University of Illinois

	<u>No. of Copies</u>
11. Air Force Materials Laboratory RTD Wright-Patterson Air Force Base Dayton, Ohio 45433 MAN 1 Copy MANC 1 Copy MAAE 1 Copy MAAM 1 Copy MAT 1 Copy MATC 1 Copy	6
12. Plastics Technical Evaluation Center Picatinny Arsenal Dover, New Jersey 07801	1
13. Defense Materials Information Center Battelle Memorial Institute 505 King Avenue Columbus, Ohio 43201	1
14. Army Materials and Mechanics Research Center Watertown, Massachusetts 02172	1
15. Directorate of Research and Engineering Watervliet Arsenal Watervliet, New York 12189	1
16. Technical Information Center Kidde Aero-Space Division Walter Kidde and Co., Inc. Belleville, New Jersey 07109	1
17. Alleghany Ballistics Laboratory Cumberland, Maryland 21502	1
18. Aerojet General Corporation P. O. Box 1947 Sacramento, California 95809	2
19. Defense Ceramic Information Center Battelle Memorial Institute 505 King Avenue Columbus, Ohio 43201	1

Distribution List for Contract N000 19-71-C-0323with Department of Theoretical and Applied Mechanics, University of Illinois

	<u>No. of Copies</u>
20. Solar Aircraft Co. 2200 Pacific Highway San Diego, California 92112 Attention: Dr. A. G. Metcalfe	1
21. Professor John Outwater University of Vermont Burlington, Vermont 05401	1
22. Hughes Aircraft Co. Aerospace Group R & D Division Culver City, California 90130	1
23. General Electric Co. Manufacturing Engineering Services One River Road Schenectady, New York 12305	1
24. A. O. Smith Co. Milwaukee, Wisconsin 53201	1
25. Mr. W. Cox Dr. S. Brelant Aerojet-General Corporation P. O. Box 296 Azusa, California 91702	1
26. IIT Research Institute Technology Center 10 West 35th Street Chicago, Illinois 60616	1
27. Owens-Corning Fiberglas Corporation (Mr. R. J. Weaver) 806 Connecticut Avenue, N. W. Washington, D. C. 20015	1
28. PPG Industries 7801 Norfolk Avenue Room 201 Bethesda, Maryland 20014	1

Distribution List for Contract N000 19-71-C-0323with Department of Theoretical and Applied Mechanics, University of Illinois

	<u>No. of Copies</u>
29. Grumman Aerospace Corp. Bethpage, L. I., New York 11714 Attention: Materials Dept.	1
30. Vought Aeronautics Division LTV Aerospace Corp. P. O. Box 5907 Dallas, Texas 75222 Attn: R. S. Rembert, Group 2-5922	1
31. Mc Donnell Douglas Astronautics Co. Advanced Manufacturing Technology 3000 Ocean Park Boulevard Santa Monica, California 90406 Attention: George Martin	1
32. Mc Donnell Douglas Astronautics Co. Materials Department 3000 Ocean Park Boulevard Santa Monica, California 90405	1
33. Goodyear Aerospace Corporation (Mr. R. A. Burkeley, Dept. 481) 1210 Massillon Road Akron, Ohio 44315	1
34. Avco Corporation (Undersea Projects Directorate) 201 Lowell Street Wilmington, Massachusetts 01887	1
35. Union Carbide Plastics Co. (Mr. A. S. Burhans) P. O. Box 670 River Road, Bound Brook New Jersey 08805	1
36. Reinforced Plastics Division Minnesota Mining and Manufacturing Co. 2501 Hudson Road St. Paul, Minnesota 55119	1
37. NASA Scientific and Technical Information Facility P. O. Box 33 College Park, Maryland 20740	1

Distribution List for Contract N000 19-71-C-0323

with Department of Theoretical and Applied Mechanics, University of Illinois

	<u>No. of Copies</u>
38. Prof. F. McGarry Massachusetts Institute of Technology Cambridge, Massachusetts 02139	1
39. Space Sciences Laboratory General Electric Co. P. O. Box 8555 Philadelphia, Pennsylvania 19101	1
40. Avco Corporation Lowell Industrial Park Lowell, Massachusetts 01851	1
41. Arthur D. Little, Inc. Acorn Park Cambridge, Massachusetts 02140 Attention: Stephen L. Kaplan	1
42. Dr. Robert R. Stromberg National Bureau of Standards Washington, D. C. 20234	1
43. Research Department Dow Corning Corporation Midland, Michigan 48640 Attention: Dr. O. K. Johansson	1
44. NASA Headquarters Washington, D. C. 20546 Attention: N. Mayer (RV-2) B. Achhammer (RRM)	2
45. Lewis Research Center NASA 21000 Brookpark Road Cleveland, Ohio 44135 Attention: Materials and Structures Div. Chemical Systems Division Liquid Rocket Technology Branch	3
46. HITCO 1600 W. 135th Street Gardena, California 90249	1

Distribution List for Contract N000 19-71-C-0323

with Department of Theoretical and Applied Mechanics, University of Illinois

	<u>No. of Copies</u>
47. Jet Propulsion Laboratory California Institute of Technology 4800 Oak Grove Drive Pasadena, California 91103 Attn: R. A. Boundy, Materials Section	1
48. Chief Materials and Processes Aerospace Group Space Division The Boeing Company P. O. Box 3707 Seattle, Washington 98124	1
49. Union Carbide Corporation Silicones Division P. O. Box 44 Tonawanda, New York 14152 Attention: San Sterman	1
50. Deep Submergence Systems Project 6900 Wisconsin Avenue Bethesda, Maryland 20034	1
51. Aero Structures Department Naval Air Development Center Warminster, Pennsylvania 18974 Attn: J. Minecci	1
52. Union Carbide Corporation Carbon Products Division Parma Research Center Technical Information Center P. O. Box 6116 Cleveland, Ohio 44101	1
53. Prof. L. Broutman Illinois Institute of Technology Chicago, Illinois 60616	1
54. P. R. Mallory and Co., Inc. 3029 E. Washington Street Indianapolis, Indiana 46206	1
55. Union Carbide Corporation Materials Systems Division Technical Library P. O. Box 24166 Indianapolis, Indiana 46224	1

Distribution List for Contract N000 19-71-C-0323

with Department of Theoretical and Applied Mechanics, University of Illinois

	<u>No. of Copies</u>
56. Research Center General Precision Inc. 1150 McBride Avenue Little Falls, New Jersey 07424 Attention: Dr. J. L. Rutherford	1
57. Plastics and Packaging Laboratory Feltman Research Laboratory Picatinny Arsenal Dover, New Jersey 07801 (Attn: Mr. Bodnar)	1
58. Naval Air Systems Command Washington, D. C. 20360 Attention: AIR-604 (Incl. 15 for DDC)	17
59. Dr. A. Kremheller Department 72-14 Zone 402 Lockheed-Georgia Company Marietta, Georgia 30060	1
60. TRW Equipment Laboratories TRW Inc. 23555 Euclid Avenue Cleveland, Ohio 44117	1
61. Hercules Research Center Wilmington, Delaware 19899 Attention: J. T. Paul	1
62. Bell Telephone Laboratories, Inc. Murry Hill, New Jersey 07971 Attention: R. Sabia	1
63. Prof. James L. Lubkin Department of Civil Engineering Michigan State University East Lansing, Michigan 48823	1
64. University of California Forest Products Laboratory 1301 South 46 Street Richmond, California 94801 Attention: J. Marian	1

Distribution List for Contract N000 19-71-C-0323with Department of Theoretical and Applied Mechanics, University of Illinois

	<u>No. of Copies</u>
65. Narmco R & D Division Whittaker Corporation 3540 Aero Court San Diego, California 92123	1
66. General Dynamics P. O. Box 748 Fort Worth, Texas Attn: Materials Dept.	1
67. Mc Donnell Douglas Corporation St. Louis, Missouri 63166 Attn: Material & Processes Development	1
68. General Technologies Corporation 1821 Michael Faraday Drive Reston, Virginia 22070	1
69. Advanced Materials R & D Martin Marietta Corporation P. O. Box 5837 Orlando, Florida 32805 Attn: Dr. Wm. F. Stuhrke	1
70. Naval Air Development Center Code MAPC Warminster, Pa. 18974 Attention: Lawrence C. Ritter Research Chemist	1